Cellular Oncology 26 (2004) 319–327
IOS Press

Optical computed-tomographic microscope for three-dimensional quantitative histology

Ravil Chamgoulov *, Pierre Lane and Calum MacAulay
Cancer Imaging Department, BC Cancer Research Centre, Vancouver, Canada

Abstract. A novel optical computed-tomographic microscope has been developed allowing quantitative three-dimensional (3D) imaging and analysis of fixed pathological material. Rather than a conventional two-dimensional (2D) image, the instrument produces a 3D representation of fixed absorption-stained material, from which quantitative histopathological features can be measured more accurately. The accurate quantification of these features is critically important in disease diagnosis and the clinical classification of cancer. The system consists of two high NA objective lenses, a light source, a digital spatial light modulator (DMD, by Texas Instrument), an x–y stage, and a CCD detector. The DMD, positioned at the back pupil-plane of the illumination objective, is employed to illuminate the specimen with parallel rays at any desired angle. The system uses a modification of the convolution backprojection algorithm for reconstruction. In contrast to fluorescent images acquired by a confocal microscope, this instrument produces 3D images of absorption stained material. Microscopic 3D volume reconstructions of absorption-stained cells have been demonstrated. Reconstructed 3D images of individual cells and tissue can be cut virtually with the distance between the axial slices less than 0.5 μm.

Keywords: 3D imaging, computed-tomography, histology, cancer diagnosis, optical microscopy, absorption-stained

1. Introduction

With the exception of immunohistochemistry, histological techniques have changed little in the last fifty years. Yet, pathological review of biopsy sections remains the cornerstone of clinical cancer diagnosis and management. The authors estimate that pathologists world-wide analyze approximately 100 million histology sections annually (25,000 pathologists looking at an average case load of 4,000 specimens per year). It is well recognized that severe limitations imposed by classical specimen preparation and microscopy systems result in sub-optimal specimen analysis conditions. Conventional practice involves cutting 4–7 μm thick tissue sections in order to image cells that are 10–30 μm in diameter. This practice is necessary to produce crisp images with the minimal overlap between cells on a conventional transmission microscope; however, the probability of imaging intact cells is rather low. This so-called sectioning artifact introduces errors in the calculation of quantitative features, such as nuclear-to-cytoplasm ratio and DNA amount. It also makes the analysis of tissue architecture difficult in more than two dimensions.

Broadly speaking, pathologists appraise biopsy sections by examining the morphology of individual cells or cell fragments, and by assessing the cellular organization or "architecture" of the tissue. The use of specific labels, for example, stoichiometrically labeled DNA, affords the opportunity to measure the amount and distribution of the label of interest. We anticipate that as knowledge is gained from genomics and proteomics, the need for examination, localization and quantification of more specific labels will increase both in clinical practice and in research applications. The sectioning artifacts presented by thin sections will always limit these endeavors unless a means is developed to easily examine thick sections.

There have been a number of developments in computer-aided pathology in the past several decades, particularly in cytometry [17,18,21,22]. Near-monolayer preparations and automated image analysis (e.g., Tripath FocalPoint) have greatly advanced cytological specimen analysis and impacted the practice of clinical cytopathology. The optical computed-tomographic (CT) microscope for 3D quantitative analysis, presented in this paper, possesses the potential to produce similar advances in both tissue (histological) and cell

*Corresponding author: Ravil Chamgoulov, Cancer Imaging Department, BC Cancer Research Centre, 601 West 10th Avenue, Vancouver, BC, Canada V5Z 1L3. Tel.: +1 604 708 4278; Fax: +1 604 708 4279; E-mail: rchamgou@bccrc.ca.

cluster (cytological) specimens, and eliminate some of the barriers to computer-aided pathology caused by thin sections. The intended clinical benefits include the ability for pathologists to: (i) look at multiple levels of a section without physical sectioning by microtome; (ii) remove sectioning artifacts caused by thin microtome slices and cell fragments; (iii) look at more natural tissue architecture, including whole intact cells.

The optical CT microscope [2,14,13], recently developed by our group at the BC Cancer Research Centre, is a novel imaging device for the 3D visualization and quantitative analysis of the internal structure of absorption-stained biological samples. A conventional optical microscope produces a 2D magnified image of a thin tissue section. 3D image acquisition of absorption-stained thick sections would allow the visualization of both 3D tissue structure and 2D virtual projections free from sectioning artifacts. The spatial arrangement of individual cells and their cellular components in 3D space is available for pathologists with the optical CT microscope. This new information may help in the earlier diagnosis of cancer.

Confocal microscopy [20] has improved our knowledge of cell and tissue structure by producing excellent 3D images of thick tissue sections. However, confocal microscopy has limitations. In general, confocal microscopy requires fluorescence stains for imaging. The bulk of pathologists' work involves interpretation of absorbance stained specimens, and there are archival and stability issues with fluorescent stained specimens. Further, the optical CT microscope represents a cost-effective alternative to confocal microscope, which can cost several hundred thousand dollars per instrument. Building on pathologists' extensive knowledge and experience derived from classical 2D absorbance microscopy, histopathology could easily shift to 3D analysis of cellular structures and tissues using quantitative 3D absorbance imaging.

The optical CT microscope employs a tomographic reconstruction technique for 3D image generation. It is an optical analogue of the well-established X-ray absorption computed-tomography technique [5,8,23]. In X-ray CT, the 3D spatial distribution of an object's linear attenuation coefficient is reconstructed from projections through the sample recorded at different angles. Mathematically, each element in the recorded projection corresponds to a line integral of the attenuation coefficient, which represents the total attenuation of the X-ray beam as it goes along a straight line through the sample. The concept of computed tomography was employed later in X-ray phase contrast tomography [1,25] and X-ray micro-tomography [19, 24].

Relatively little attention has been given to straight-ray tomographic techniques in the context of optical microscopy. The idea of tomographic optical microscopy using a computerized reconstruction algorithm and a transmission optical microscope was first proposed by S. Minami and S. Kawata at Osaka University (Japan) in 1985. Their first system was a straight implementation of the X-ray computed-tomography technique in an optical microscope. The group used a mechanical rotation system to illuminate the sample at different angles. Over a five-year period the group published a series of papers [10,9,16], in which they discussed their research results and algorithms for tomographic reconstruction.

2. Optical computed-tomography microscope with digital light modulator

Our group was the first to use a spatial light modulator in an optical CT microscope [4,3,15]. The group in collaboration with Digital Optical Imaging Corp. has built a bench-top instrument with a digital micromirror device (DMD, by Texas Instruments Inc.) as the spatial light modulator in order to control the angles of light rays that illuminate a sample [2]. The DMD is an array of tiny micromirrors (on 17 μm centres), each of which can be controlled individually (Fig. 1). An aperture displayed on the DMD at some position (x, y) causes the specimen to be illuminated at a specific angle (ϕ, θ). Figure 2 illustrates the coordinate system. The polar angle ϕ is the angle between the optical axis Z and the direction of illumination light rays. The azimuthal angle θ is the angle between the X-axis and the projection of the light ray in the XY plane.

Using the DMD instead of a mechanical rotation system provides considerable advantages in flexibility, speed, and precision. It enables computer-controlled sequential illumination and detection with an appointed set of illumination angles. Instead of mechanically rotating, or tilting the specimen, the system allows changing electronically the angles of light rays for illumination of a stationary specimen.

The DMD can be used as a spatial light modulator for different types of microscopes. Papers published by our and other research groups describe an application of the DMD for confocal microscopy [12,7,6] and confocal microendoscopy [11]. However, in this paper we present a different type of microscope: opti-

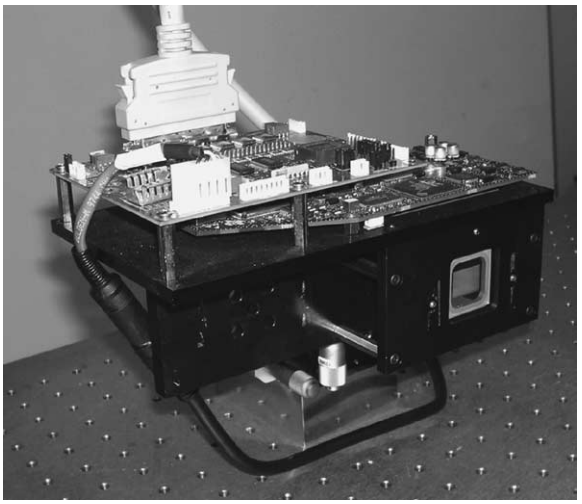

Fig. 1. Digital Micromirror Device (or DMD by Texas Instruments Inc.). The array of micromirrors is visible in the front, while the control system is on the top. The size of the array is 17.4 mm × 13.1 mm. It consists of 1024 × 768 micromirrors.

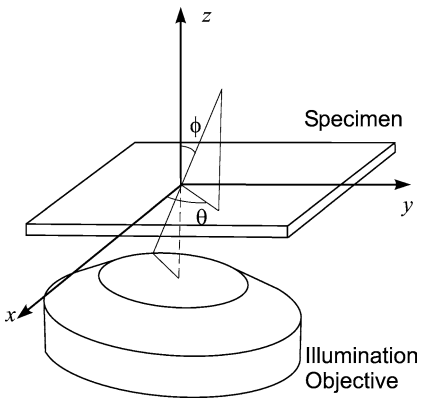

Fig. 2. The coordinate system. Z-axis corresponds to the optical axis of the microscope. The polar angle ϕ is the angle between the optical axis Z and the direction of illumination light rays. The polar angle $-\phi_{\max} \leqslant \phi < \phi_{\max}$ is limited by the numerical aperture of the objective. The azimuthal angle θ is the angle between the X-axis and the projection of the light ray in the XY plane. Azimuthal angle could be any angle $0 \leqslant \theta < 2\pi$, constant for a particular set of projections.

cal computed-tomographic microscope for absorption-stained biological samples imaging.

A schematic of the optical CT microscope based on the DMD is presented in Fig. 3. The instrument is based on a conventional transmission microscope in which the sub-stage condenser has been replaced with a second objective lens mounted on its own independent translation stage. The system consists of two high-numerical aperture objective lenses, relay lenses, a DMD, a light source, and a CCD camera. The field stop limits the illuminated field of view at the specimen. The DMD is placed in the illumination path of the microscope conjugate to the back pupil plane of the illumination objective (condenser lens). The system aperture stop is located at the DMD. This aperture stop is projected into the back pupil plane (conjugate aperture stop) of the objective by a relay lens. The DMD determines which part of the back pupil plane receives illumination. A circular disk of "on-mirrors" (30–50 micromirrors in diameter) written to the DMD serves as an off-axis aperture stop. The position of the disk on the DMD corresponds to a particular angle of illumination. As the disk is translated across the DMD, the angle of illumination changes accordingly. The primary (image-forming) and secondary (illumination) objectives were identical (Zeiss PlanApo 63×-1.4NA oil). The resolution of the DMD was 1024 × 768 micromirrors with an on-off contrast ratio of 255 : 1. The specimen was mounted between two large cover slips and placed on the microscope stage. A picture of the DMD-based optical computed-tomographic microscope is shown in Fig. 4. The system provides the ability to acquire projections from any arbitrary azimuthal angle, $0 \leqslant \theta < 2\pi$. The maximal theoretical polar angle $-\phi_{\max} \leqslant \phi < \phi_{\max}$ was limited by the numerical aperture (NA) of the objective lens to $\pm 67.5°$. In practice we used projections within $\pm 60°$ due to the finite solid angle subtended by the illumination disk.

The limited angle constraint is a critical limitation of the computed-tomographic microscopy system that must be overcome using the proper reconstruction algorithm. Another limitation is related to absorption. If too much light is absorbed by the specimen, the acquisition time is too long. To decrease the absorption we reduced the staining time during specimen preparation. Scattering that may cause serious problems in some macroscopic applications like optical mammography, does not seem to be a problem at the microscopic level, at least for specimen thickness up to 20 μm. To date, we have not investigated how thicknesses more than 20 μm affect the reconstruction quality.

3. Reconstruction of 3D images

3.1. Reconstruction algorithm

The filtered back-projection algorithm [8] that combines information from different angular positions can calculate the 3D distribution of the attenuation coeffi-

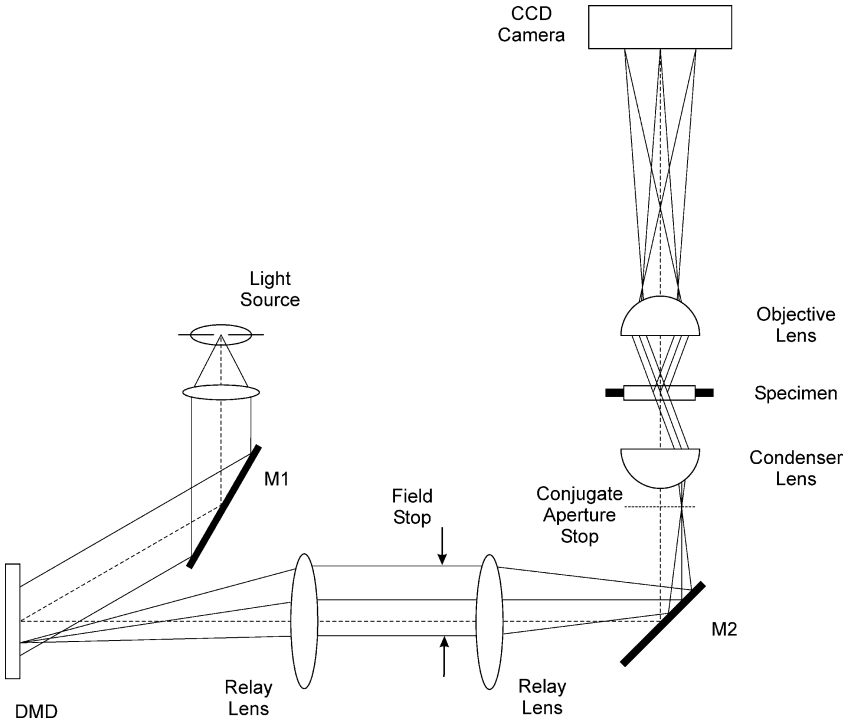

Fig. 3. Schematic of the DMD-based optical computed-tomographic microscope.

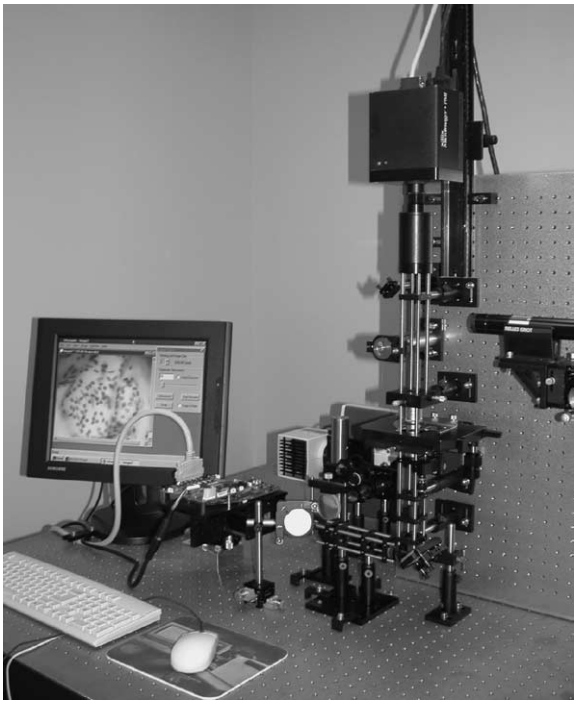

Fig. 4. DMD-based optical computed-tomographic microscope.

cient in the absorption stained sample. Since the attenuation coefficient is directly proportional to a density for a given material, the technique effectively allows the determination of the three-dimensional density distribution in the sample. The filtered back-projection algorithm is currently used in almost all applications of straight ray tomography. It has been shown to be very accurate and amenable to fast implementation. Briefly, the gray scale values of the image are converted from absorption units to an optical density. Each pixel from the optical-density image is projected back through a reconstruction volume. This volume acts as a 3D array of accumulators. The accumulated optical density at each voxel produces a 3D volume representation of the specimen.

Filtering of images is needed during the reconstruction in order to correct for blurring effects. Filtering and back projection are both linear operations, and they can be performed in any order. However, it is better to perform the filtering before the back projection since this involves fewer computations. We performed filtering of images in a frequency domain by multiplying the Fourier transform of a projection by the filter's transfer function. The result was then inverse Fourier transformed to produce the filtered image. A number of different types of filters were tested in our computer

simulations. The Shepp–Logan filter, which combines a sinc function with a ramp filter, was chosen for our application since it was less sensitive to noise and resulted in a small amount of blurring.

The reconstruction algorithm developed by our group, involves reconstruction from several sets of projections made from different directions of illumination scanning, and combination of several reconstructions in order to compensate for incompleteness of information due to the limited NA of the optical system. The limited NA in the CT microscope is a major problem for traditional reconstruction techniques. It leads to the presence of artifacts in the reconstructed image and image distortion. In order to improve the quality of images in a final reconstruction and to remove the distortion, the final 3D object was generated from several reconstructions of the object made from different azimuthal angles. The spatial light modulator that we used in the system enabled us to obtain several sets of object projections acquired from different directions of illumination. A single reconstruction data set was acquired by illuminating the sample with light at different polar angles, $\phi_1 \leqslant \phi < \phi_2$, and constant azimuthal angle θ. This data set, and its corresponding reconstructed volume, are referred to as have being "acquired along direction θ". A composite reconstruction is assembled from several single reconstructions acquired along multiple directions. Voxels from different reconstructions were combined using four different methods: average, minimum, maximum, and median vote criteria. The median vote method seemed to work the best. Finally, our 3D reconstruction algorithm, which was validated with experimental data, can be described in the following basic steps:

- Acquire initial 2D images of a sample (projections, taken under different angles with a CCD camera). The images are cropped, centered and corrected using usual image non-uniform illumination correction algorithm.
- Corrected images are converted into a set of sinograms. The "sinogram" of a projected image is the collection of all possible line-projections through the image. (One single projection measures the attenuated beam intensity, and thus the line integral of the attenuation coefficient along projected rays.)
- The sinograms are digitally filtered. The inverse Radon transform is performed to backproject the sinograms and produce a reconstructed slice of the 3D object.
- A 3D reconstructed volume is created from a stack of reconstructed slices.
- Several reconstructions of the same object are combined together to compensate the incompleteness of information due to the limited angular field of view.

3.2. *Microscopic 3D image reconstruction results and discussion*

In our research we used formalin-fixed, paraffin-embedded lung specimens. The tissue sections were cut at thickness from 4 to 20 μm. Two different staining methods were used: Feulgen-Thionin, and Hematoxylin + Eosin (H&E). The Feulgen-Thionin staining method was modified by reducing the staining time from one hour to 7 minutes, at room temperature. H&E staining was performed according to laboratory standards.

One to four sets of projections were measured with the CCD camera for every final reconstruction. Each set consisted of ether 121, or 65 projections of a specimen, and projections were uniformly distributed within angular interval 120°. Two CCD images of a Feulgen-Thionin stained biopsy sample acquired at two different illumination angles are shown in Fig. 5. The size of acquired CCD images was 648×516 pixels. The acquisition time was 0.8 sec per image. For reconstruction all initial CCD images were cropped to the area of interest (usually 256×256 pixels).

Microscopic 3D volume reconstructions of quantitatively absorption-stained cells have been demonstrated. A reconstructed volume was commonly created as a cube with the size of $256 \times 256 \times 256$ voxels. The computational time was about 2 sec per reconstructed slice. The reconstruction algorithm was coded in Matlab for ease of implementation. Coding in C language could reduce the reconstruction time considerably. An example of the reconstructed volume is presented in Fig. 6(a–h). The figure illustrates a z-axis image-stack of Feulgen-Thionin stained thick tissue specimen. The z-axis separation between images in the figure is 1–2 μm. The image-stack was virtually sliced from a 3D reconstructed volume, generated from two sets of projections that were taken from two different azimuthal angles, and polar angles $-56° \leqslant \theta \leqslant 56°$. Every set included a total of 57 projections (8 of the 65 projections were removed for this particular reconstruction). Reconstructed 3D images of individual cells and tissue can be cut virtually with the distance between the axial slices less than 0.5 μm. The X, Y and

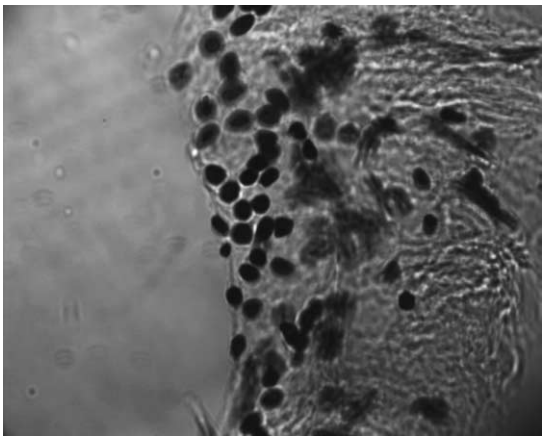

(a)

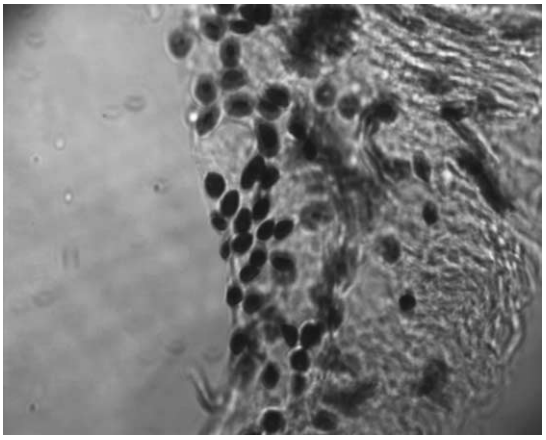

(b)

Fig. 5. Two projections (a) and (b), acquired at two different illumination angles. The relative angle between (a) and (b) is 64 degrees. Sample of biopsy is stained with Feulgen-Thionin to show DNA content.

Z resolution is sufficient to see the inner cellular structure. To date, we have not measured the resolution of the system.

The optical CT microscope possesses the ability to make the results of quantitative 3D imaging comparable to 2D analysis by virtual slicing and projection of reconstructed 3D biological samples. Virtual cutting and virtual slicing of 3D reconstructed volumes can provide valuable information for pathological interpretation and diagnosis. A virtual slice can include a layer with totally intact cells, and a 2D projection from such a slice will have all the quantitative information of intact cells and will be presented in the way convenient for pathological interpretation with known methods. Algorithms for virtual slicing, segmentation, and projection of reconstructed 3D biological objects are under development.

Architectural analysis of pathological material can also be performed based on the quantitative information acquired by the optical CT microscope. For cancer diagnosis, architectural analysis attempts to characterize neoplastic progression at the level of tissue organization, i.e., measuring the organization of cells within the tissue. With this technique, the position of cell nuclei is determined for each cell in the region of interest, and a tessellation (i.e., tiling) of the image is performed. The density of cells and the thickness of the epithelium can be computed. The orientation of cells with respect to the basement membrane can be investigated. Up to 20 features may be extracted from graphical representations of the cell positions. In analogy with descriptions of order in crystalline structures, the entropy (degree of disorder) and other properties of the spatial distribution of cells may be defined and the local and global extent of cell clustering may be quantified. The spatial distribution of reconstructed cells is illustrated in Fig. 7(a–h), where a rotation of a reconstructed tissue-biopsy in 3D space is shown. Additional 3D reconstructions and image-stacks can be viewed online at www.bccrc.ca/optical-tomography/.

The optical CT method is easily extended for multicolor imaging by the sequential illumination of the sample with red, green, and blue light. A feasibility of generating 3D true-color RGB (red-green-blue) images was demonstrated with optical CT microscope.

4. Conclusion

A novel optical computed-tomographic microscope has been developed based on digital light modulation technology for image projections acquisition and the radon-transform-based method for reconstruction of 3D images. The algorithm combines information from different angular positions to calculate a distribution of the attenuation coefficients in the specimen. The system provides the ability to acquire projections from any arbitrary azimuthal angle $0 \leqslant \theta < 2\pi$, and the polar angle theoretically limited to $-67.5^\circ \leqslant \phi \leqslant 67.5^\circ$.

The optical CT microscope has demonstrated the feasibility of 3D histological analysis of absorption stained tissue. The instrument can provide additional 3D diagnostic information to pathologists that might be critical for cancer detection and diagnosis. The optical CT microscope overcomes the limitations of confocal microscopy, which is expensive, and re-

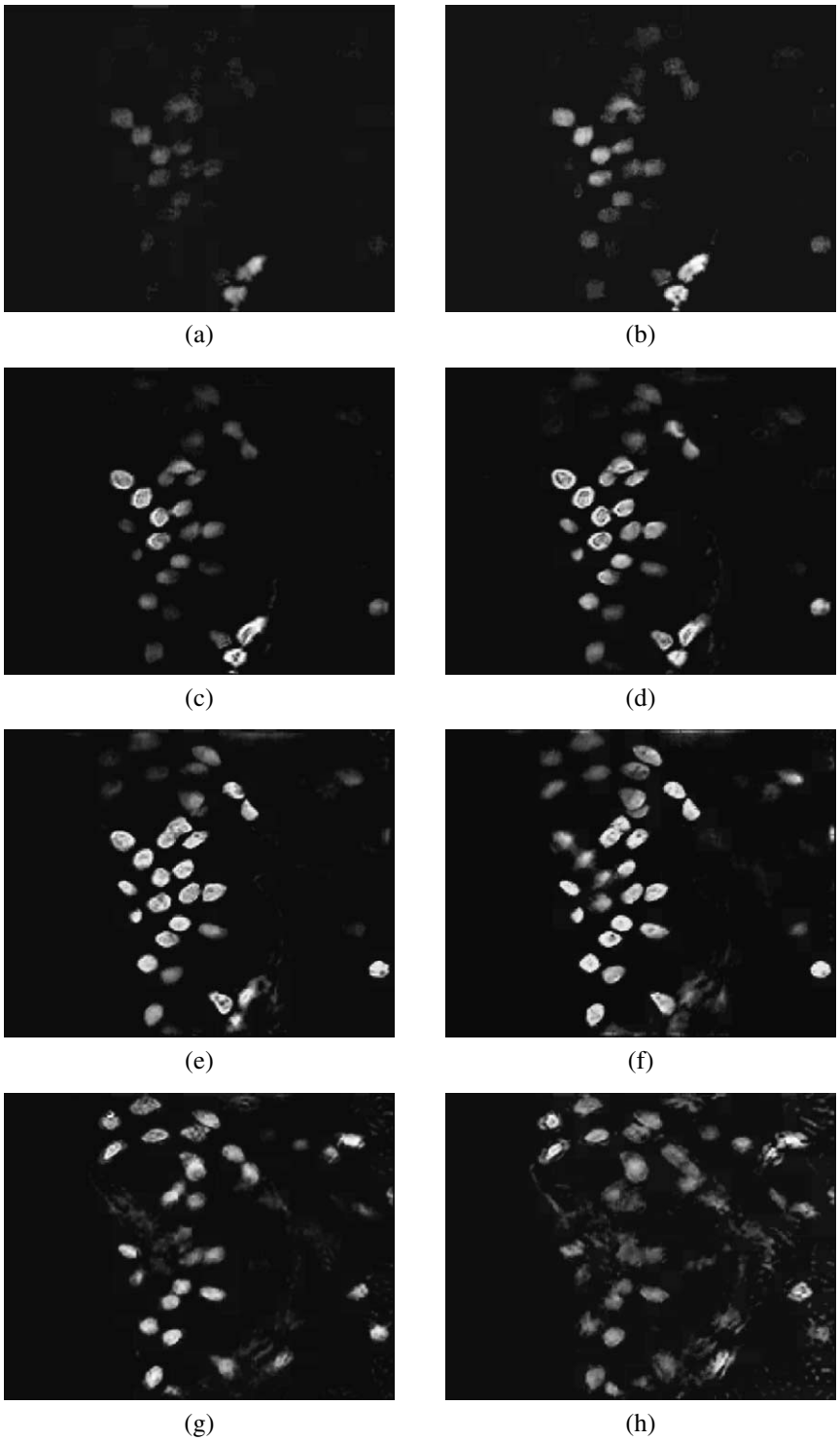

Fig. 6. Z-axis image-stack of Feulgen-Thionin stained thick tissue specimen. The z-axis separation between images is 1–2 μm. The image-stack was virtually sliced from a 3D reconstruction, generated from 57 projections acquired over 112°. The images are shown in optical density units where black pixels correspond to zero absorption and white pixels correspond to maximum absorption.

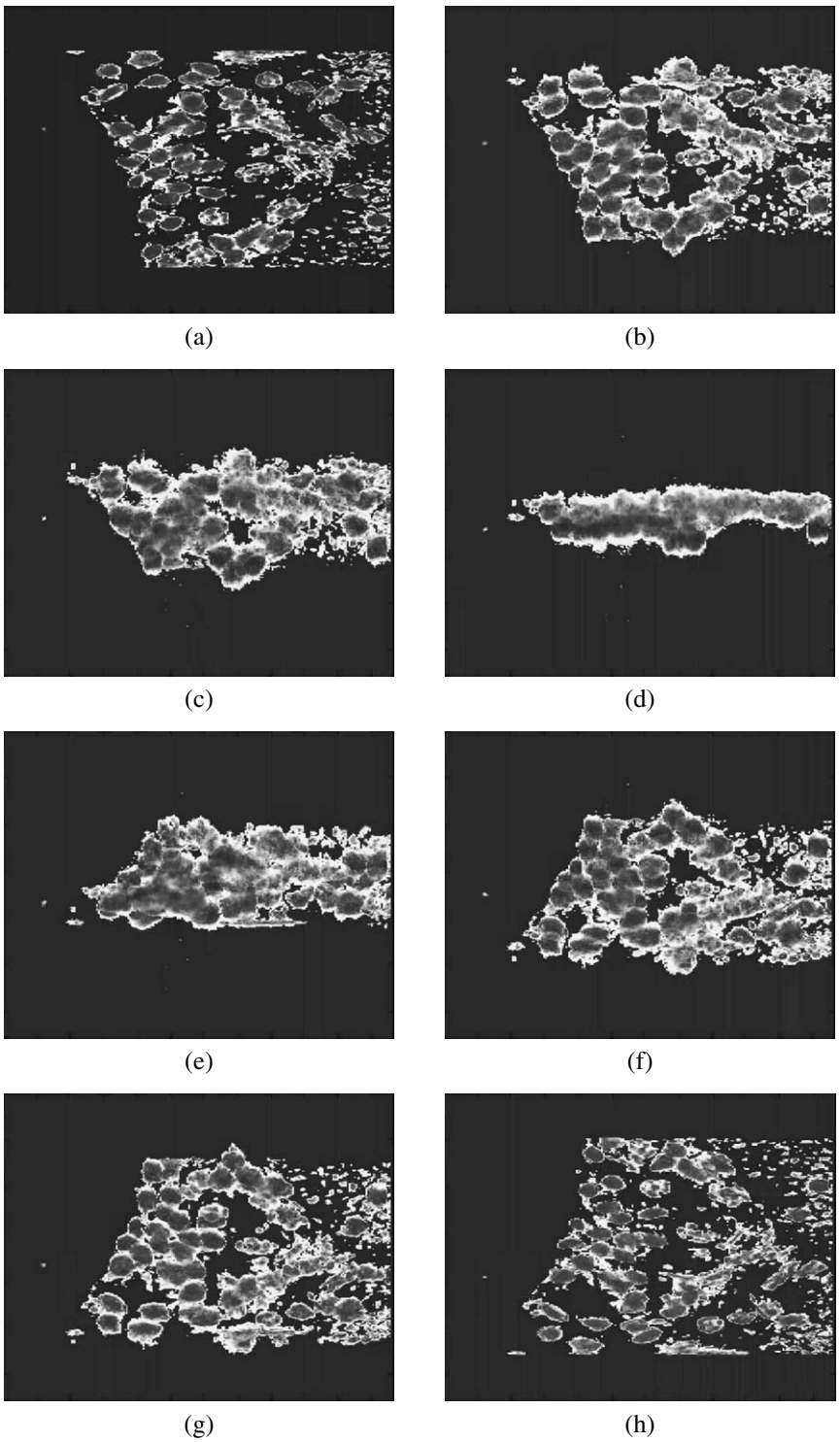

Fig. 7. The figures (a–h) illustrate a rotation of a 3D reconstructed tissue-biopsy. The angle between each view (a) through (d) is approximately 20 degrees. (d) corresponds to the angle of view perpendicular to the glass slide.

quires fluorescent stained material. Microscopic 3D volume reconstructions of quantitatively absorption-stained cells have been demonstrated.

The instrument enables pathologists to look at multiple optical levels of a section with the distance between virtual slices less than 0.5 μm. More natural tissue architecture, including whole intact cells, and a spatial arrangement of individual cells and their cellular components, are available for analysis with the optical CT microscope. The optical computed-tomographic microscope enables to acquire 3D images of thick tissue sections, 20 μm or more, where numerous intact cells are presented.

Acknowledgement

This work was supported by a grant (MOP-15349) of the Canadian Institute of Health Research (CIHR).

References

[1] A. Barty, K.A. Nugent, A. Roberts and D. Paganin, Quantitative phase tomography, *Optics Communications* **175** (2000), 329–336.

[2] R.O. Chamgoulov, P.M. Lane, A.L.P. Dlugan and C.E. MacAulay, Optical microscopic tomography with digital spatial light modulator, in: *Proceedings of IASTED International Conference Biomedical Engineering*, 2003, pp. 89–94.

[3] A.L.P. Dlugan, C.E. MacAulay and P.M. Lane, Improvements to quantitative microscopy through the use of digital micromirror devices, *Proc. SPIE* **3921** (2000), 6–11.

[4] A.L.P. Dlugan and C.E. MacAulay, Update on the use of digital micromirror devices in quantitative microscopy, *Proc. SPIE* **3404** (1999), 253–262.

[5] J.G. Fujimoto et al., Optical coherence tomography: an emerging technology for biomedical imaging and optical biopsy, *Neoplasia* **2** (2000), 9–25.

[6] T. Fukano and A. Miyawaki, Whole-field fluorescence microscope with digital micromirror device: imaging of biological samples, *Applied Optics* **42**(19) (2003), 4119–4124.

[7] Q.S. Hanley, P.J. Verveer, M.J. Gemkow, D. Arndt-Jovin and T.M. Jovin, An optical sectioning programmable array microscope implemented with a digital micromirror device, *Journal of Microscopy* **196**(Pt. 3) (1999), 317–331.

[8] C. Kak and M. Slaney, *Principles of Computerized Tomographic Imaging*, Society of Industrial and Applied Mathematics, Philadelphia, 2001.

[9] S. Kawata, The optical computed tomography microscope, in: *Advances in Electron and Optical Microscopy*, T. Mulvey and C.J.R. Sheppard, eds, Vol. 14, Academic, London, 1994, pp. 213–248.

[10] S. Kawata, Y. Touki and S. Minami, Optical microscopic tomography, *Proc. SPIE* **558** (1985), 15–20.

[11] P.M. Lane, A.L.P. Dlugan and C.E. MacAulay, Digital micromirror device (DMD) enabled confocal microendoscopy, *Proc. SPIE* **4251** (2001), 192–198.

[12] P.M. Lane, A.L.P. Dlugan, R. Richards-Kortum and C.E. MacAulay, Fiber-optic confocal microscopy using a spatial light modulator, *Optics Letters* **25** (2000), 1780–1782.

[13] C. MacAulay, R. Chamgoulov, A. Dlugan and P. Lane, Micromirror devices in cellular microscopy, Abstract #O.19, *International Conference on Applied Genomics – 9th ESACP/16th ISDQP Meeting (ICAG-2003)*, Amsterdam, The Netherlands, 2003.

[14] C.E. MacAulay, Apparatus and methods relating to spatially light modulated microscopy, United States Patent 6,483,641, 2002.

[15] C.E. MacAulay and A.L.P. Dlugan, Use of digital micro mirror devices in quantitative microscopy, *Proc. SPIE* **3260** (1998), 201–206.

[16] O. Nakamura, S. Kawata and S. Minami, Optical microscopic tomography. II. Nonnegative constraint by a gradient-projection method, *J. Opt. Soc. Am. A* **5** (1988), 554–561.

[17] C. Ortiz De Solorzano, S. Costes, D.E. Callahan, B. Parvin and Barcellos-Hoff, Applications of quantitative digital image analysis to breast cancer research, *Microscopy Research and Technique* **59** (2002), 119–127.

[18] B. Palcic, D.M. Garner, J. Beveridge, X.R. Sun, A. Doudkine, C. MacAulay, S. Lam and P.W. Payne, Increase of sensitivity of sputum cytology using high-resolution image cytometry: field study results, *Cytometry (Clinical Cytometry)* **50** (2002), 168–176.

[19] S.J. Pan, W.S. Liou, A. Shih, M.S. Park, G. Wang, S.P. Newberry, H. Kim, D.M. Shinozaki and P.C. Cheng, Experimental system for X-ray cone-beam microtomography, *Microscopy Microanalysis* **4** (1998), 56–62.

[20] J.B. Pawley, ed., *Handbook of Biological Confocal Microscopy*, 2nd edn, Plenum Press, New York, 1995.

[21] F. Schnorrenberg, C.S. Pattichis, K. Kyriacou, M. Vassiliou and C.N. Schizas, Computer-aided classification of breast cancer nuclei, *Technology and Health Care Journal* **4**(2) (1996), 147–161.

[22] R. Swartz, L. West, I. Boiko, A. Malpica, C. MacAulay, A. Carraro, M. Guillaud, D. Cox and M. Follen, Use of nuclear morphometry characteristics to distinguish between normal and abnormal cervical glandular histologies, *Analytical Cellular Pathology* **25**(4) (2003), 193–200.

[23] P.J. Tadrous, Methods for imaging the structure and function of living tissues and cells: I. Optical coherence tomography, *J. Pathol.* **191** (2000), 115–119.

[24] G. Wang, T.H. Lin, P.C. Cheng, D.M. Shinozaki and H.-G. Kim, Scanning cone-beam reconstruction algorithms for X-ray microtomography, *Proc. SPIE* **1556** (1999), 99–112.

[25] C. Yang, A. Wax, R. Dasari and M. Feld, Phase-dispersion optical tomography, *Optics Letters* **26**(10) (2001), 686–688.